Developments in Atmosphere Revitalization Modeling and Simulation

James C. Knox, Kenneth Kittredge, Robert F. Coker, Ramona Cummings, and Carlos F. Gomez
NASA Marshall Space Flight Center, Huntsville, Alabama, 35812, USA

"NASA's Advanced Exploration Systems (AES) program is pioneering new approaches for rapidly developing prototype systems, demonstrating key capabilities, and validating operational concepts for future human missions beyond Earth orbit" (*NASA 2012*). **These forays beyond the confines of earth's gravity will place unprecedented demands on launch systems. They must not only blast out of earth's gravity well as during the Apollo moon missions, but also launch the supplies needed to sustain a crew over longer periods for exploration missions beyond earth's moon. Thus all spacecraft systems, including those for the separation of metabolic carbon dioxide and water from a crewed vehicle, must be minimized with respect to mass, power, and volume. Emphasis is also placed on system robustness both to minimize replacement parts and ensure crew safety when a quick return to earth is not possible. Current efforts are focused on improving the current state-of-the-art systems utilizing fixed beds of sorbent pellets by evaluating structured sorbents, seeking more robust pelletized sorbents, and examining alternate bed configurations to improve system efficiency and reliability. These development efforts combine testing of sub-scale systems and multi-physics computer simulations to evaluate candidate approaches, select the best performing options, and optimize the configuration of the selected approach, which is then implemented in a full-scale integrated atmosphere revitalization test. This paper describes the development of atmosphere revitalization models and simulations. A companion paper discusses the hardware design and sorbent screening and characterization effort in support of the Atmosphere Revitalization Recovery and Environmental Monitoring (ARREM) project within the AES program.**

I. Nomenclature

a	saturation capacity in Toth equation, mol kg^{-1} kPa^{-1}
a_0	Toth equation parameter, mol kg^{-1} kPa^{-1}
a_f	superficial free flow area, m^2
a_w	column cross-sectional area, m^2
b	equilibrium constant in Toth equation, kPa^{-1}
b_0	Toth equation parameter, kPa^{-1}
c	concentration, mol m^{-3}: also parameter in Toth equation, K
c_o	inlet concentration, mol m^{-3}
c_{pg}	gas heat capacity, J kg^{-1} K^{-1}
c_{ps}	sorbent heat capacity, J kg^{-1} K^{-1}
c_{pw}	column wall heat capacity, J kg^{-1} K^{-1}
h_{sg}	sorbent to gas heat transfer coefficient, W m^{-2} K^{-1}

D_L	axial dispersion coefficient, $m^2\ s^{-1}$
E	Toth equation parameter, K^{-1}
h_{wg}	column wall to gas heat transfer coefficient, $W\ m^{-2}\ K^{-1}$
h_{wa}	column wall to ambient heat transfer coefficient, $W\ m^{-2}\ K^{-1}$
k_g	gas conduction, $W\ m^{-1}\ K^{-1}$
k_m	mass transfer coefficient, s^{-1}
k_s	sorbent conduction, $W\ m^{-1}\ K^{-1}$
k_w	column wall conduction, $W\ m^{-1}\ K^{-1}$
L	bed height, m
n	sorbent loading, $mol\ kg^{-1}$
p	partial pressure in Toth equation, kPa
Pe	particle Peclet number
P_i	column inner perimeter, m^2
P_o	column outer perimeter, m^2
$\overline{q}$	average adsorbed concentration, $mol\ m^{-3}$
q^*	equilibrium adsorption concentration, $mol\ m^{-3}$
R_p	pellet radius, m
t	time, seconds; also heterogeneity parameter in Toth equation
t_0	Toth equation parameter
T_g	gas temperature, K
T_s	sorbent temperature, K
T_w	column wall temperature, K
T_0	inlet temperature, K
x	axial coordinate, m
∂H	differential heat of adsorption, $kJ\ mol^{-1}$
ε	void fraction
ε_w	void fraction at the column wall
v_i	interstitial velocity, $m\ s^{-1}$
dL	gas density, $kg\ m^{-3}$
ρ_s	sorbent density, $kg\ m^{-3}$

ρ_w	column wall density, kg m^{-3}
D_w	Distance to nearest wall, m
G	Inverse of distance to nearest wall = $1/D_w$, m^{-1}
σ_w	diffusion coefficient in Eikonal (distance to wall) equation
P^{H2O}	Partial pressure of water vapor, Pa
κ	Permeability, m^2
Q	Heating source due to sorption, W m^{-3}
β_F	Forchheimer coefficient, kg m^{-4}
R_i	Reaction rate, mol m^{-3} s^{-1}
C	Void scaling
ε	Porosity
ε_∞	ideal perfectly packed porosity (e.g., without the Al mesh)
m	Bed mass, g
R	Bed internal diameter, mm
l	Column wall thickness, mm
A_L	Langmuir surface area, m^2 g^{-1}
μ	Dynamic viscosity, Pa-s
ε_m	Volume fraction taken up by Al mesh
η	Sorption efficiency

II. Introduction

Predictive simulation tools are being developed to reduce the hardware testing requirements of the Atmosphere Revitalization Recovery and Environmental Monitoring (ARREM) project. Although sub-scale testing is required to establish the predictive capability of the simulation, the much greater cost of extensive full-scale testing can be limited to that required for the confirmation of analytical design optimization studies. Non-recurring costs of predictive simulation development are non-trivial, however, once predicative capability is established, geometric reconfiguration of a model is straightforward. A predictive simulation capability provides numerous additional benefits. Understanding of complex processes is greatly increased since process conditions (temperature, pressure, concentrations,

etc.) may be examined anywhere in the adsorption column. Weaknesses in a prototype design can be readily identified and improvements tested via simulation. Finally, the predictive simulation provides a powerful tool for virtual troubleshooting of deployed flight hardware.

III. Development of Fixed Bed Modeling Approach

Adsorption in fixed beds of pelletized sorbents is the primary means of gas separation for atmosphere revitalization systems. For the bulk separation of CO_2 and H_2O, temperature changes due to the heat of adsorption are significant, requiring the modeling and simulation of the heat balance equations. For columns with small tube diameter to pellet diameter ratios, as encountered in internally heated columns, flow channeling along the column wall can have a strong influence on overall performance. In some cases, the influence is great enough to necessitate the use of 2-D simulations.

Breakthrough tests, where a regenerated column is challenged with a constant inlet of sorbate and carrier gas, are used to determine mass transfer coefficients via empirical correlation. The mass transfer coefficient for a sorbate/sorbent pair may then be used to simulate cyclic, regenerative adsorption processes of interest. The development of fixed bed models and verification using breakthrough test results is described below.

A. Experimental

Data from fixed bed testing (Mohamadinejad, Knox and Smith 2000) conducted at NASA's Marshall Space Flight Center (MSFC) was used to develop and verify fixed bed models in the COMSOL multi-physics simulation package. This test stand had a unique capability where gas concentration was captured not only far downstream of the fixed bed but also along the fixed bed centerline in three locations (inlet, midpoint, and endpoint). Temperatures were also captured at the same locations as shown in Fig 1. The difference between the exit concentration at the axial center the concentration after mixing provides valuable insight into non-ideal flow behaviors such as channeling along the wall and axial dispersion, which we will see are difficult to capture in 1-D adsorption models for certain sorbate/sorbent systems. Table 1 provides the properties of the adsorbent and fixed bed used to develop and validate the appropriate modeling approaches to support AES ARREM CO_2 removal design studies.

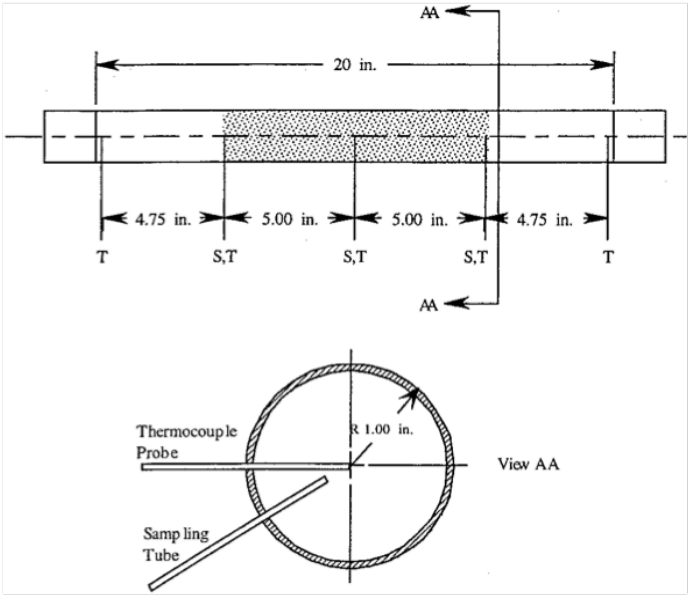

Figure 1. Breakthrough Test Apparatus. *The fixed bed test section is the center 10 inches of the column.*

Table 1. Properties of the adsorbent and fixed bed

Adsorbent		Fixed-bed	
Pellet radius	R_p = 1.02 mm	Bed height	L = 0.254 m
Particle density	ρ_s = 1180 kg m^{-3}	Bed mass	m = 396 g
Skeletal density	ρ_{sk} = 2040 kg m^{-3}	Bed internal diameter	R_i = 47.6 mm
Heat capacity	c_{ps} = 920 J kg^{-1} K^{-1}	Column wall thickness	l = 1.59 mm
Langmuir surface area	A_L = 463 m^2 g^{-1}	Wall heat capacity	c_{pw} = 475 J kg^{-1} K^{-1}
		Wall density	ρ_w = 7833 kg m^{-3}

B. 1-D Model

One-dimensional models are favored for speed and simplicity in fixed-bed simulations. However, in some cases, higher dimensions must be used to attain a sufficient accuracy in simulation results. This is illustrated in the results sections below.

1. 1-D Mathematical Model

Equations implemented in the COMSOL PDE General Form physics mode for the 1-D model are summarized below. The following assumptions were used in the derivation of these equations:

- All mechanical dispersion effects are lumped together with molecular diffusion in the axial dispersion term.
- Plug flow is assumed, i.e., there is no gradient of velocity, concentration, temperature, or porosity in the radial direction.
- Velocity in the axial direction is not compensated for loss of sorbate since the sorbate gas mole fraction is << 1.
- Velocity is temperature compensated via the ideal gas law.

Gas Phase Mass Balance

$$\frac{\partial c}{\partial t}+\left(\frac{1-\varepsilon}{\varepsilon}\right)\frac{\partial \overline{q}}{\partial t}-D_L\frac{\partial^2 c}{\partial x^2}=-\upsilon_i\frac{\partial c}{\partial x} \tag{1}$$

Gas Phase B.C.

$$-D_L\left.\frac{\partial c}{\partial x}\right|_{x=0}=\upsilon_i(c_o-c)\qquad \left.\frac{\partial c}{\partial x}\right|_{x=L}=0 \tag{2}$$

Sorbent Mass Balance

$$\frac{\partial \overline{q}}{\partial t}=k_m(q^*-\overline{q}) \tag{3}$$

Heat Balance

$$\varepsilon a_f\rho_g c_{pg}\frac{\partial T_g}{\partial t}-\varepsilon a_f k_g\frac{\partial^2 T_g}{\partial x^2}=-\varepsilon a_f\rho_g\upsilon_i c_{pg}\frac{\partial T_g}{\partial x}+a_s h_{sg}\left(T_s-T_g\right)+\varepsilon_w P_i h_{wg}\left(T_w-T_g\right) \tag{4}$$

Heat Balance B.C.

$$-k_g\left.\frac{\partial T_g}{\partial x}\right|_{x=0}=-\rho_g\upsilon_i c_{pg}\left(T_0-T_g\right)\qquad \left.\frac{\partial T_g}{\partial x}\right|_{x=L}=0 \tag{5}$$

Sorbent Heat Balance

$$a_f\rho_s c_{ps}\frac{\partial T_s}{\partial t}-a_f k_s\frac{\partial^2 T_s}{\partial x^2}=a_s h_{sg}\left(T_g-T_s\right)-a_f\partial H\frac{\partial q}{\partial t} \tag{6}$$

Column Heat Balance

$$a_w \rho_w c_{pw} \frac{\partial T_w}{\partial t} - a_w k_w \frac{\partial^2 T_w}{\partial x^2} = \varepsilon_w P_i h_{wg} \left(T_g - T_w\right) + P_o h_{wa} \left(T_a - T_w\right) \quad (7)$$

Toth Isotherm

$$n = \frac{ap}{\left[1 + (bp)^t\right]^{1/t}}; \quad b = b_0 \exp(E/T); \quad a = a_0 \exp(E/T); \quad t = t_0 + c/T \quad (8)$$

Axial Dispersion Coefficient

$$\frac{1}{Pe_2} = \frac{0.73\varepsilon}{\mathrm{Re}\, Sc} + \frac{1}{2\left(1 + \frac{13 \cdot 0.73\varepsilon}{\mathrm{Re}\, Sc}\right)} \quad 0.0377 < 2R_p < 0.607 \text{ cm} \quad (9)$$

2. Results and Discussion: Breakthrough Tests and 1-D Simulations for Carbon Dioxide on Zeolite CaA

Figure 2 provides the concentration history and temperature history respectively for breakthrough tests and 1-D simulation results with carbon dioxide on zeolite CaA. Note that the mass transfer coefficient k_m is treated as a fitted parameter. The concentration comparison is quite favorable for the Mixed concentration, which is the desired result for a 1-D model. The temperature comparison is also quite favorable; although the peak temperature is slightly higher, the point in time when the simulated temperature begins to decrease closely matches test data, indicating properly timing of the simulated adsorption front.

A comparison of the experimental Exit and Mixed concentrations in Fig. 2 reflect the influence of channeling at the wall of the column, where packing density is lower allowing greater velocity and earlier saturation. Since the average flow rate is higher than that at the centerline of the column, the Mixed data (reflecting the average concentration for the column) breaks through earlier than the Exit data (reflecting the centerline concentration).

The plug flow 1-D model cannot capture cross-flow velocity gradients evident in this data. The axial dispersion term was varied from the value representing molecular diffusion to the highest value provided by standard correlations, yet has negligible effect on the simulation results. Nonetheless, for the CO2/zeolite CaA system, the simulation provides a good representation of adsorption physics and is suitable for use in development studies.

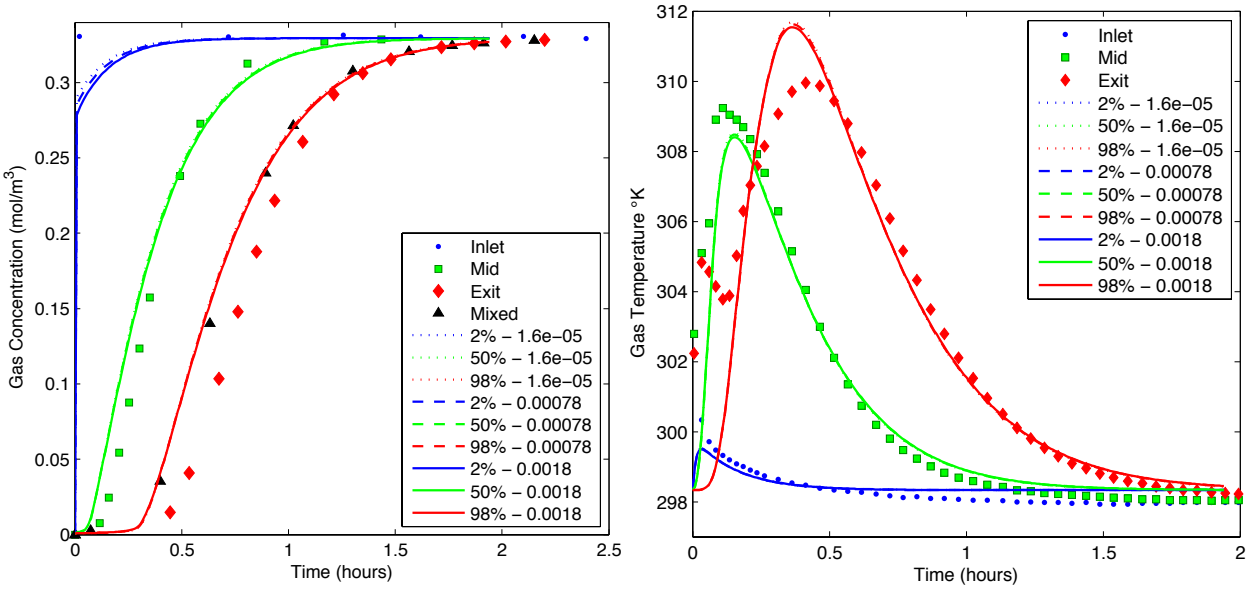

Figure 2. Breakthrough test data and 1-D simulation results for CO_2 on zeolite CaA. *Concentration history (left) and temperature history (right). Experimental data are shown as symbols. Simulation data at the inlet (2%), midpoint (50%), and exit (98%) are shown as lines. Three values for axial dispersion (units are $m^2\ s^{-1}$) are compared in these figures, however, their influence is negligible on simulation results.*

3. Results and Discussion: Breakthrough Tests and 1-D Simulations for Water Vapor on Zeolite CaA

Figure 3 provides the concentration history and temperature history respectively for breakthrough tests and 1-D simulation results with water vapor on zeolite CaA. Once again the mass transfer coefficient k_m is treated as a fitted parameter. Additionally, the void fraction was varied for better visual comparison of the test and simulated breakthrough curves. For the H_2O/zeolite CaA system, is was not possible to simulate the Mixed concentration data as in the CO_2/zeolite CaA system with the 1-D model. Zeolite CaA has a much greater affinity for water then CO2 resulting in much longer time before breakthrough. This provides more time for the effect of channeling to propagate down the column as evidenced by the increased gap between the Mixed concentration (diamonds) and Exit concentration (squares).

Although the comparison of test and simulated concentrations at the column midpoint and exit is favorable, the desired result for design studies is the mixed concentration. The comparison of test and simulated temperatures is much less favorable: the later drop in temperature in the simulation indicates that the simulation is not capturing the timing of the adsorption process well.

The data presented here indicates that the 1-D simulation of the H_2O/zeolite CaA system is non-conservative and not sufficiently accurate for design studies. 2-D axisymmetric models under development for this purpose are described next; these include the variations of porosity near the column wall.

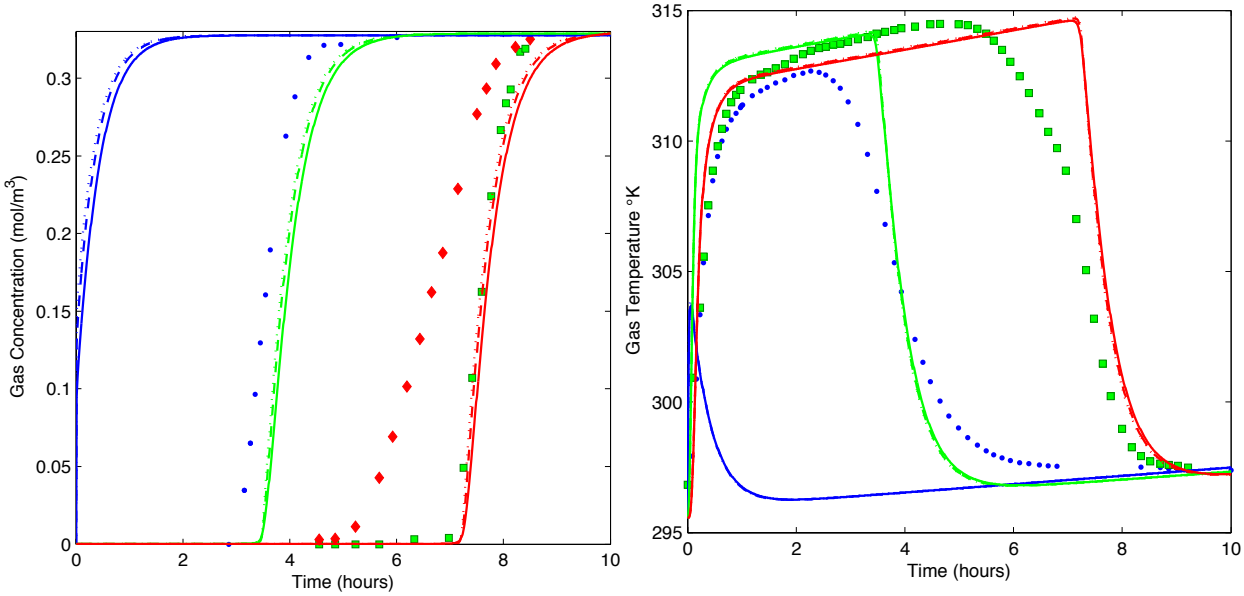

Figure 3. Breakthrough test data and 1-D simulation results for H_2O on zeolite CaA. *Concentration history (left) and temperature history (right). Experimental data are shown as symbols. Simulation data at the inlet (2%), midpoint (50%), and exit (98%) are shown as lines. Three values for axial dispersion (units are $m^2\ s^{-1}$) are compared in these figures, however, their influence is negligible on simulation results.*

C. 2-D Axisymmetric Model

The COMSOL 2-D axisymmetric model was constructed using four physics modes.

1. 2-D Axisymmetric Mathematical Model

Equations from the four COMSOL physics modes utilized in this simulation are shown below. Detailed information on the origin of these equations may be found in the COMSOL User Guide (COMSOL 2009).

• Free and Porous Media Flow, including Darcy and Forchheimer terms (Eq. (10))

$$\frac{\rho_g}{\varepsilon}\left(\frac{\partial \vec{u}_i}{\partial t}+\left(\vec{u}_i\cdot\nabla\right)\frac{\vec{u}_i}{\varepsilon}\right)=\nabla\cdot\left[-pI+\frac{\mu}{\varepsilon}\left(\nabla\vec{u}_i+\nabla\vec{u}_i\right)^T-\frac{2\mu}{3\varepsilon}\left(\nabla\cdot\vec{u}_i\right)I\right]-\left(\frac{\mu}{\kappa}+\beta_F\left|u_i\right|\right)\vec{u}_i$$

$$\frac{\partial\left(\varepsilon\rho_g\right)}{\partial t}+\nabla\cdot\left(\rho_g\vec{u}_i\right)=0 \qquad (10)$$

• Transport of Diluted Species (Eq. (11))

$$\frac{\partial c}{\partial t} + \nabla \cdot \vec{N} = R_i$$

$$\vec{N} = -D_L \nabla c + \vec{u}_i c \tag{11}$$

- Distributed ODEs and DAEs (adsorbent mass balance; same as Eq. (3))
- Heat Transfer (Eq. (12))

$$(\rho C_p)_{EQ} \frac{\partial T_g}{\partial t} + \rho_g c_{pg} \vec{u}_i \cdot \nabla T_g = \nabla \cdot (k_{EQ} \nabla T_g) + Q \tag{12a}$$

$$(\rho C_p)_{EQ} = (1-\varepsilon)\rho_s c_{ps} + \varepsilon \rho_g c_{pg} \tag{12b}$$

$$k_{EQ} = (1-\varepsilon)k_s + \varepsilon k_g \tag{12c}$$

Porosity variation is accounted for in Eq. (13), where y is the distance to the wall

$$\varepsilon = \varepsilon_\infty \left[1 + C \exp\left(-N \frac{y}{d_p} \right) \right] \text{with } N = 2...8 \text{ and } C = \frac{1}{\varepsilon_\infty - 1} \tag{13}$$

2. 2-D Axisymmetric Results and Discussion

Using Eq. (13) to account for the porosity variation near the wall with $N = 4$, the CO_2/zeolite CaA system was simulated, with the results shown in Fig. 4 and 5. The porosity variation arises from the lack of pellet nestling near the canister wall. It is evident in Fig. (4) that the inclusion of the porosity effect in the simulation results in a faithfully capturing both the mixed and centerline concentrations. This approach is preferred for the CO_2/zeolite CaA system when higher accuracy is desired, although at the cost of greatly increased computational time.

It was shown earlier that the 1-D approach is does not provide acceptable simulation results for the H_2O/zeolite CaA system. The 2-D axisymmetric approach is also being developed for this system; due to the higher numerical stiffness of this system, there are convergence issues which must be resolved.

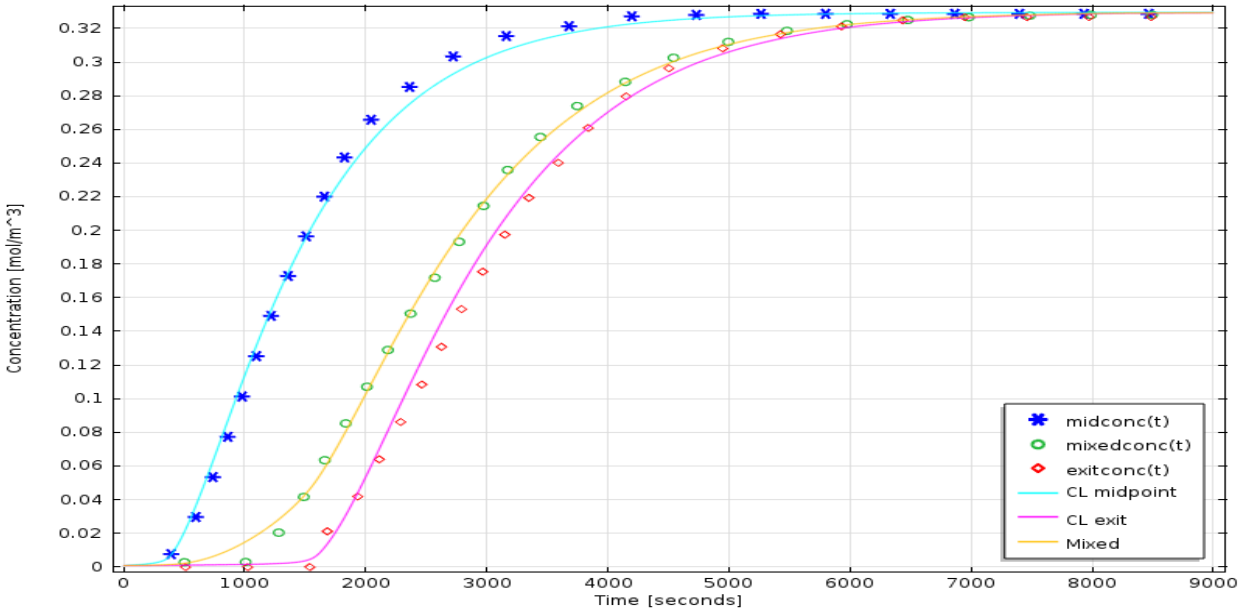

Figure 4. Breakthrough test concentration data and 2-D axisymmetric simulation results for CO_2 on zeolite CaA.

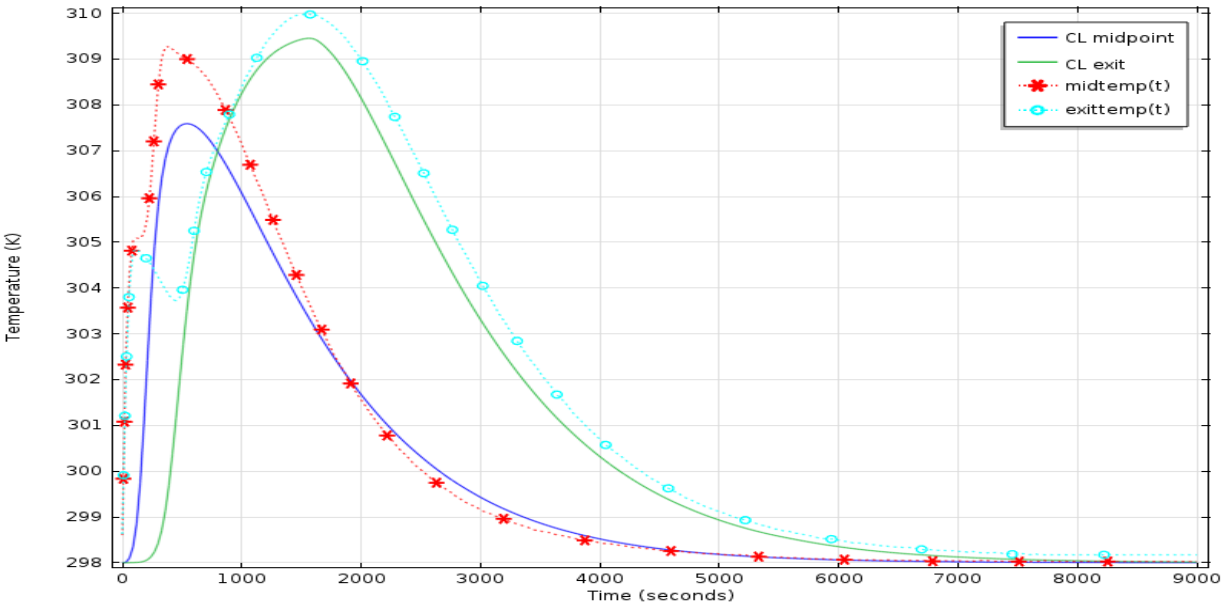

Figure 5. Breakthrough test temperature data and 2-D axisymmetric simulation results for CO_2 on zeolite CaA.

IV. Isothermal Bulk Desiccant Development

A water-saving bulk drying stage prior to downstream AR trace contaminant control and CO_2 removal processes is under development by NASA. Both membrane and fixed bed approaches are under consideration. The primary goal is to continuously remove at least 80% and up to 100% of water from a process air stream. Ideally, the bulk dryer will operate without active heating during regeneration to minimize power requirements. This may be accomplished by using the dry CO_2 removal system outlet air to regenerate the bulk dryer via a purge which returns the captured water back to the cabin atmosphere. Process optimizations such as passive thermal control are of prime interest. Development of a bulk drying stage for a water-save AR process at the NASA's Marshall Space Flight Center (MSFC) has focused on a silica gel-based isothermal bulk desiccant (IBD) system with emphasis on evaluating the performance benefits of thermally linking the adsorbing and desorbing beds.

Experimental efforts to date have included (1) a 4-cell thermally linked system with silica gel sorbent and 17 liter per minute flow rate and (2) a 2-cell non-thermally linked system with silica gel sorbent and 140 liter per minute flow rate (Perry, Howard, Knox and Junaedi 2009). A mild pressure swing was applied to increase the performance of the 140 liter per minute system.

In the ARREM program, computer modeling and simulation is being used to compare process improvements via thermal linking with the additional complexity required. Two analytical efforts are described below; the first includes only the thermal balances and arbitrarily imposes the heat of adsorption in order to provide a comparison of hardware approaches for thermal linking. In the second effort, adsorption physics are explicitly modeled in 3D using an approach modified from the 2D axisymmetric approach previously described.

A. 3D Thermal Modeling and Simulation - Thermal Linking Design Trade Study

A trade study has been performed that looks at alternative designs to enhance the heat transfer between adjacent desiccant beds in a moisture removal system. The study originally focused on the use of fins running transversely between the beds and looked at the effect on performance of variation in fin spacing and thickness. The study was subsequently expanded to include designs incorporating mid-bed heat transfer blocks, metal foam and electron beam melting (EBM) lattice designs. This study looked solely at the thermal performance of the various designs and as-

sumed the adsorbing/desorbing performance was identical in all cases. The finite difference thermal analysis program, Thermal Desktop by Cullimore and Ring, was used to predict the thermal performance of the different bed designs.

1. Modeling and Simulation

The thermal model was based on 1/3 of a six bed full scale concept, incorporating 2 beds each 5.625" deep (in the flow direction), 1.5" wide and 7.5" long. Moisture laden air enters one bed at a rate of 20/3 scfm and a temperature of 80°F. Simultaneously, dry air at the same rate and temperature enters the adjacent bed but from the opposite direction. This flow scenario continues for 15 minutes, at which point the flows are switched. The simulation continues in this manner, switching every 15 minutes, until quasi-steady state conditions are achieved.

The heat of adsorption and desorption were assumed to be equal and opposite at a rate of 243.5 btu/hr per bed. This heating(cooling) was applied, in its entirety, to 1/9th bed sections for 1/9th of the half cycle time, progressing axially through the bed, in discrete 1/9th steps, in the direction of flow. Air and desiccant were assumed to be at the same temperature. Heat transfer within the bed is assumed to be via the airflow axially through the bed and at the rate of conduction through air, radially. Heat transfer to the external environment was ignored. All structure is aluminum 6061-T6.

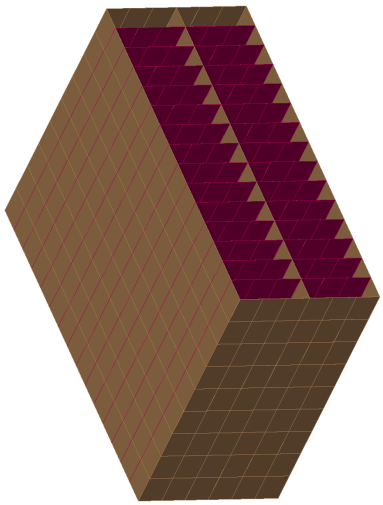

Figure 6. Fin Assessment Thermal Model

2. Results and Discussion: Fin Concepts

Thermal linking performance of fins of different spacing and thickness was assessed to determine an optimum arrangement. In all cases the fins run transversely between beds as shown in the Thermal Desktop model in Fig.6. Thermal Desktop elements were used in the fins and sidewalls so that the thicknesses could be modified without requiring the configuration to be redrawn. Fin spacings of both 0.5" and 0.25" and Fin thicknesses from 1/50" to 1/8" were assessed. Interestingly, the fin thickness had almost no effect on the temperature difference between beds. Reducing the fin spacing (increasing the number of fins) has a more significant, but still unsatisfactory effect on the bed-to-bed ΔT.

Figure 7 shows average bed temperatures during a half cycle for both beds with no fins and beds with 1/16" fins on 1/2" spacing. Decreasing the spacing to 1/4" more than triples the magnitude of the reduction in ΔT but still results in little performance improvement. It is hypothesized that the fin surface area in contact with the flow is much too small to result in significant reductions on the bed-to-bed temperature differences and the fin spacing must be greatly reduced to increase this area. Unfortunately, very small fin spacing complicates bed packing and leads to flow short-circuiting the bed thru the interstitial gaps between the fin walls and the desiccant beads.

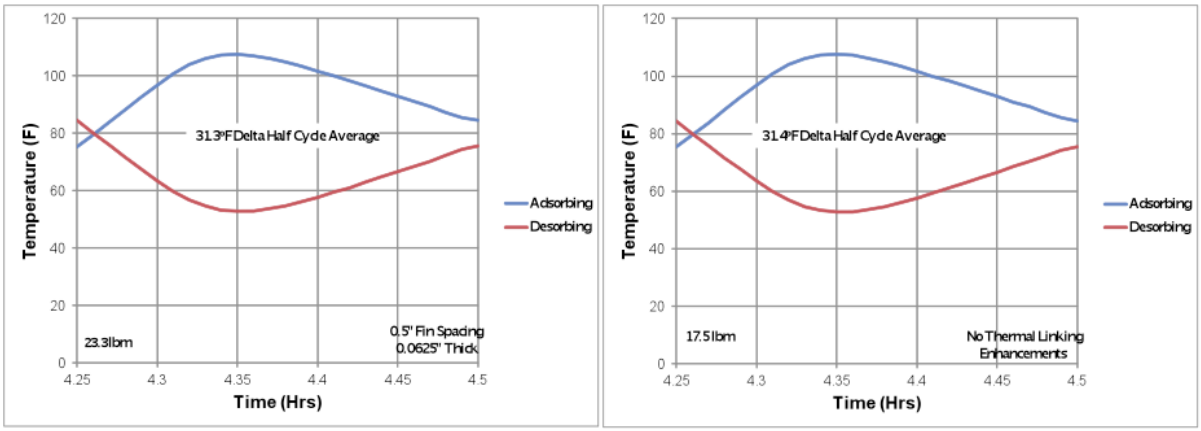

Figure 7. Effect of Fins on Temperature Difference Between Beds

3. Results and Discussion: Metal Foam

Duocel aluminum foam has been used successfully to enhance thermal linking in desiccant beds and was analyzed as part of this study. A 10 ppi, 8% density foam was chosen for this assessment because it was previously util-

ized in subscale tests at MSFC where it demonstrated significant performance in both CO_2 and moisture reduction trials. The downside was shown to be an increase in bed pressure drop caused by the reduced bead size required to fully load the bed.

The foam was modeled as porous blocks occupying the same space as the desiccant/air. Thermal parameters utilized in the model were from Duocel literature and are reproduced in Fig. 8 (ERG Aerospace Corporation). Thermal performance was vastly superior compared to fins with an average ΔT of 16°F compared with 31°F for the case of no thermal linking enhancement features. Plots of bed temperatures for a half cycle are shown in Fig. 9.

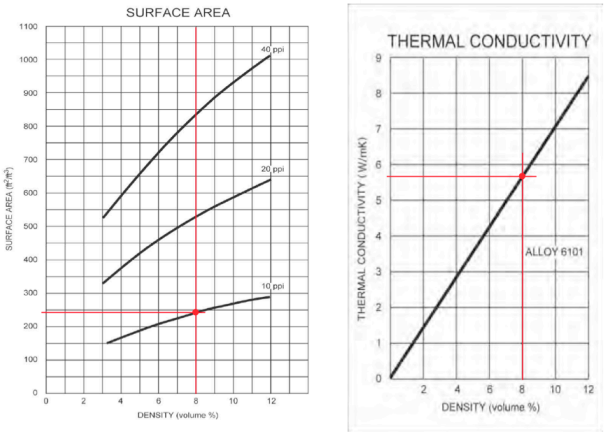

Figure 8. Duocel Aluminum Foam Data Showing Performance Point Assessed

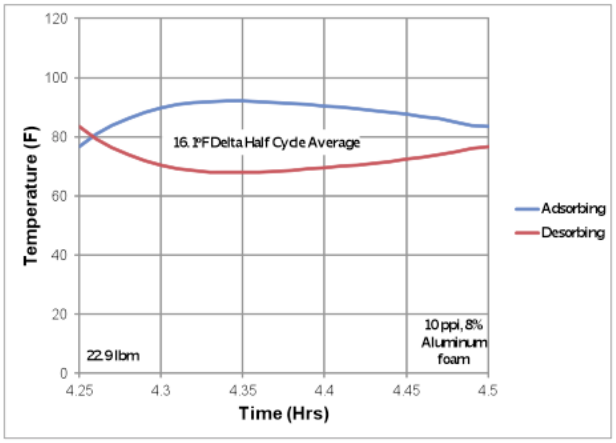

Figure 9. Effect of Aluminum Foam on Temperature Difference Between Beds

4. Results and Discussion: EBM Matrix

Advances at MSFC with electron beam melting (EBM) of aluminum provide the opportunity to generate delicate, complex structures within voids. A design of an internal matrix within the desiccant bed was generated in the hopes of retaining the overall thermal performance of the aluminum foam but with lower pressure drop and easier loading characteristics. The matrix shown in Figure 10 was the result. It consists of offset layers of 0.05" diameter strands arranged in 1/2" flat-to-flat hexagonal shapes, and spaced 1/4" apart. The matrix was first analyzed by itself to determine its thermal characteristics. This is overlaid on the Duocel foam charts in Figure 11. As is apparent in Figure 11, the EBM matrix does not have the density, conductance, or surface area of the metal foam. This is borne out in the plot in Fig. 12 where performance is seen to be little better than the non-thermal linking case.

A design was also analyzed where the strands were increased to 0.625" diameter and the hex size was reduced to 3/8" flat-to-flat. The thermal characteristics of this design are also shown in Fig. 11 and the thermal linking performance in Fig. 12. Although the density and thermal conductance are comparable to the metal foam, the surface area is much smaller and the performance is degraded because of this. In order to get the performance of the metal foam the surface area of the strands would need to be increased. This would lead to something like a star shaped cross-section or other complex geometry that have not been pursued.

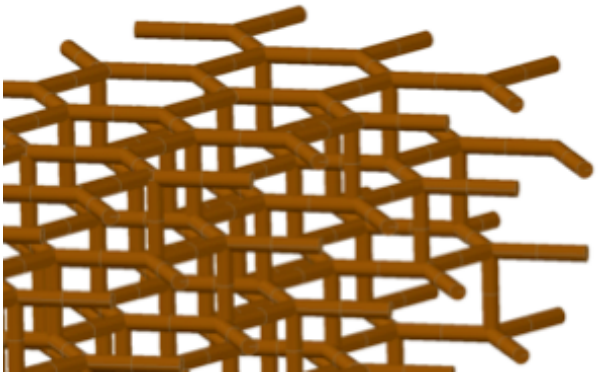

Figure 10. EBM Matrix Design
1.5" 7.5" x 5.625" Matrix; 1/2" flat-to-flat distance; 0.05" dia. strands; 1/4" spacing between layers

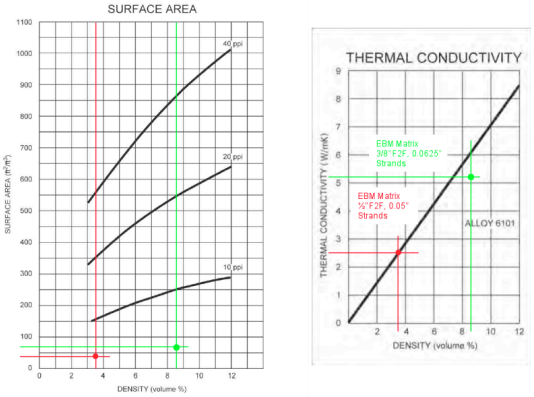

Figure 11. EBM Matrix Performance Data Superimposed on ERG Duocel Aluminum Foam

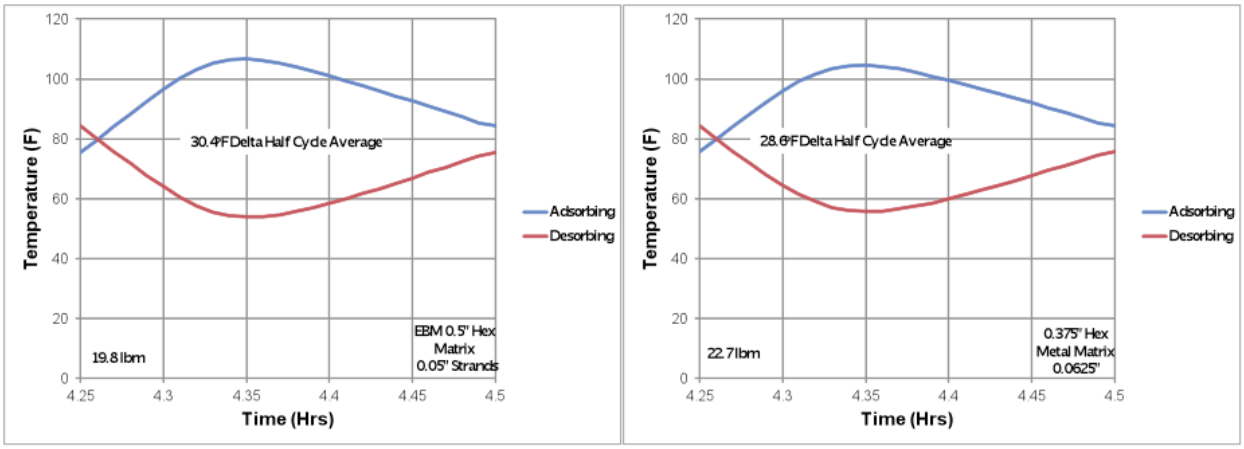

Figure 12. Effect of EBM Matrix on Temperature Difference Between Beds

5. Results and Discussion: Heat Transfer Block

The final concept assessed uses a little different philosophy. Instead of having the thermal linking and the moisture reduction/bed drying occurring in the same space, the thermal linking is separated out. To accomplish this the beds were split in half and a heat exchanger consisting of a solid aluminum block with multiple through holes was inserted in the between the bed halves. This concept is illustrated in Fig. 13. The rationale is to allow the temperature increase in the adsorbing side and temperature decrease in the desorbing side to occur up to the midpoint in the bed then have the heat exchanger essentially reset conditions back to that at the inlets.

The first design assessed consisted of a 1" thick block with 539 through holes per bed, each 0.1" in diameter. Additional cases assessing the performance of 1/2" and 1/4" blocks as well as the addition of blocks at the inlets and outlets were also analyzed. Finally, a case with 8 heat transfer blocks imbedded in the beds, each 3/32" thick was analyzed in an attempt to essentially cap the potential performance to be realized with this concept. Performance of this case is shown in Figure 14.

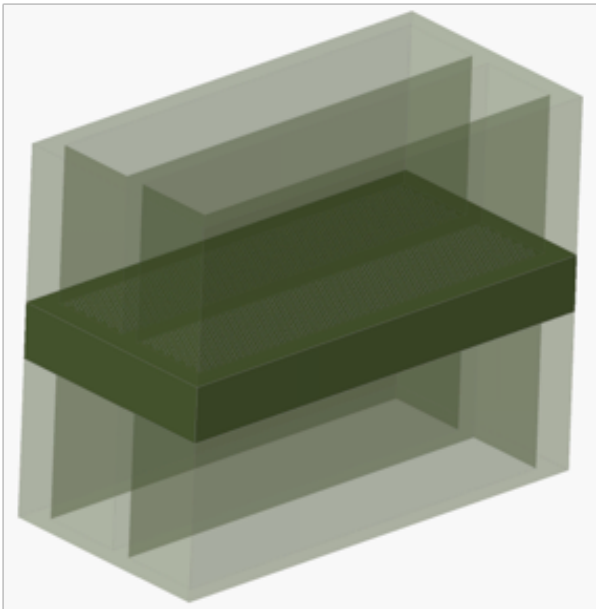

Figure 13. Heat Transfer Block Design

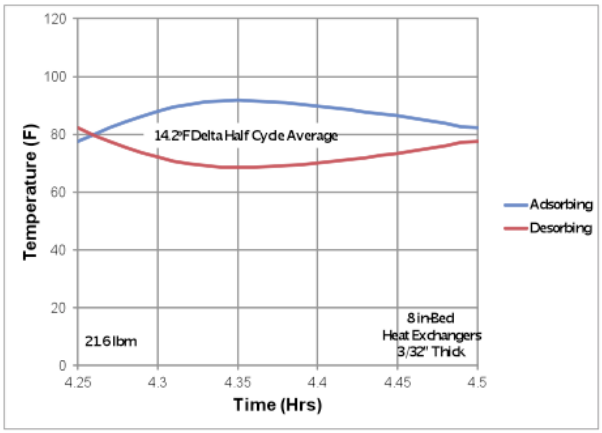

Figure 14. Performance of Eight In-Bed Heat Exchangers

6. Conclusions

All cases analyzed are displayed in Fig. 15 plotted against assumed masses. The eight bed case has significantly better performance than the rest, however, manufacturing and loading this configuration may prove challenging. A test fixture emulating the 1/3 scale bed layout that the preceding analyses have been based on has been designed and is described in a companion paper. It incorporates three 0.2" thick in-bed heat exchangers plus 0.2" thick heat exchangers at the inlets/outlets. While not yet analyzed, it is hoped that this configuration will match that of the 10 ppi aluminum foam. The cut-away solid model of this concept is shown in Fig. 16.

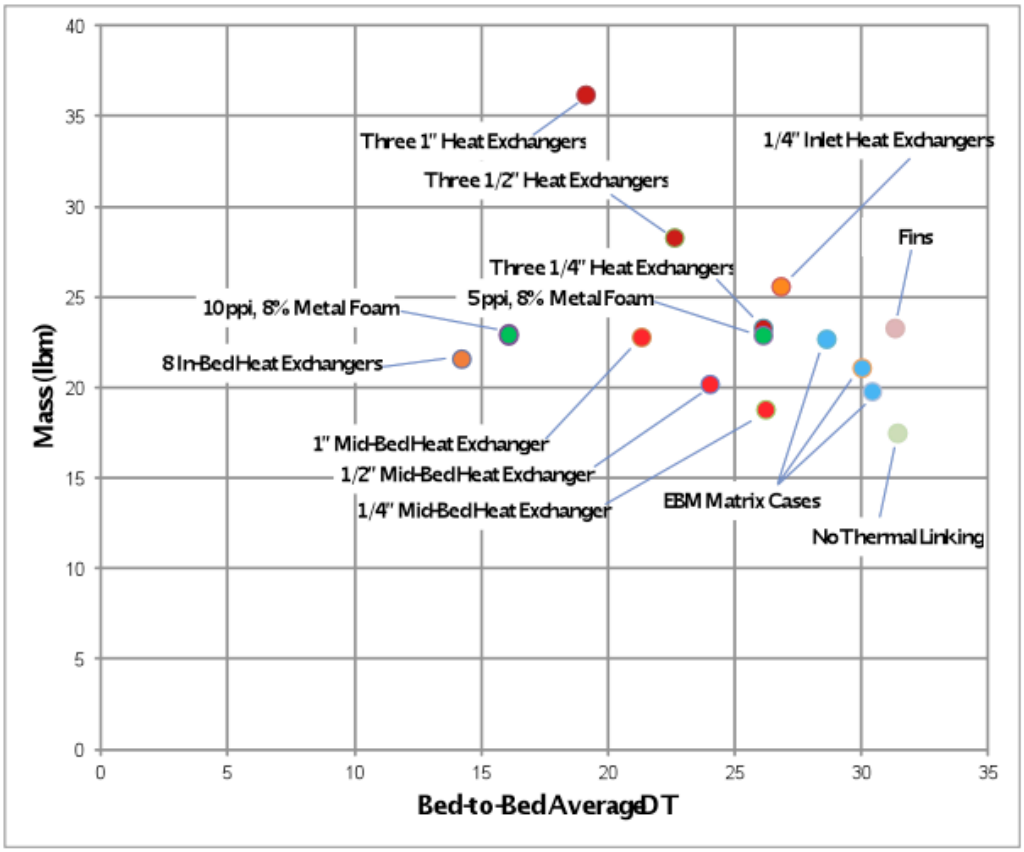

Figure 15. Performance Summary

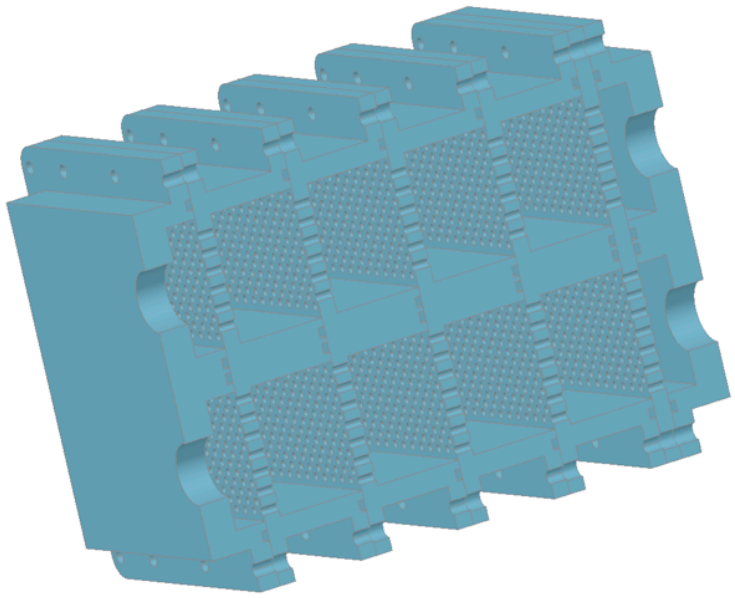

Figure 16. Cutaway of proposed Test Fixture

B. 3D Thermal Modeling and Simulation with Adsorption Physics

1. Modeling and Simulation

Initial models of the 4-column IBD with an aluminum (Al) foam lattice were conducted used the COMSOL Multiphysics code. For the porous flow part of the model, the code solves the low Mach number, compressible Brinkman equations modified by a Forchheimer drag term (Eq. 10 above). Forchheimer drag adds a drag term that is proportional to the square of the fluid velocity, rather than just linear, as is the case in Darcy flow, with a coefficient given by $\beta_F = 1.75\rho_g * \sqrt{(\varepsilon /150/\kappa)}$. Heat transfer is modeled by solving the heat transfer equations separately for the porous medium (the beds) and the solid Al holder, with appropriate boundary conditions (Eq. (11) above). For example, the holder has a heat flux boundary on its exterior based on the ambient temperature of 298.75K. The concentration of H_2O is modeled by solving a diluted species transport equation in the form of Fick's law with convection (Eq. (11) above). Since the partial pressure of H_2O is ~0.01 atm, while the system is at ~1 atm, the dilute transport assumption is valid. The

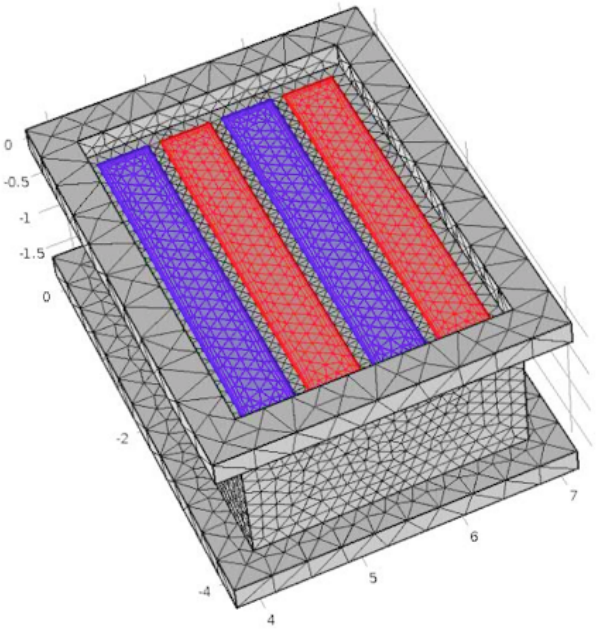

Figure 17. Meshed IBD 4-column model. *The red and blue regions are paired wet/dry inlets/exits of the columns. The size of the IBD bed in the three dimensions are shown in inches.*

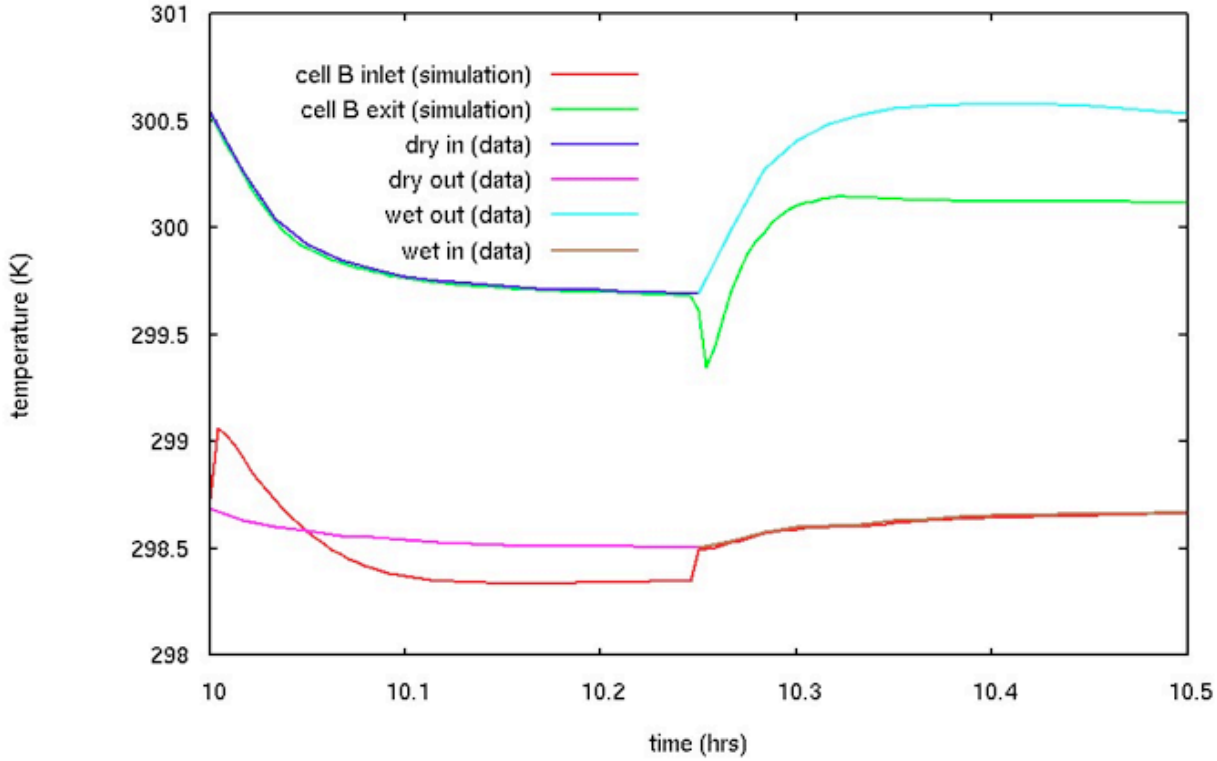

Figure 18. Temperature comparison. *The 'in' data (upper left and bottom right curves) are used as boundary conditions in the simulation. The values were taken at the center-line of the left red bed in Fig. 17, on the inlet and exit surfaces. Note the inlet and exit of cell B are spatially fixed, so that the 'inlet' is where wet air enters, but dry air exits.*

mean loading, $\bar{q}$, is modeled, via the Glueckauf approximation, with a simple ordinary differential equation given by Eq. (3) above. k is an empirically derived mass transfer coefficient and the equilibrium loading, q^*, is a function of P and T based on the Toth isotherms. The loading rate is used to determine the heat source in the porous heat transfer equation, Q, as well as the reactions in the water transport equation, R_i.

Here, $Q = -(1-\varepsilon)\frac{\partial q}{\partial t}\partial H$ and $R_i = -\frac{\partial q}{\partial t}\frac{(1-\varepsilon)}{\varepsilon}$

The carrier gas, N2, is modeled as an ideal gas with variable heat capacity, density, thermal conductivity, and viscosity. All other physical parameters (Al thermal conductivity, diffusion coefficient, etc.) are assumed to be constant except for the system's porosity and permeability. The porosity, ε, varies with location, approaching unity at the walls, and is modeled as per the Tobis and Vortmeter prescription (Eq. (13) above) with N=4, so that: $\varepsilon = \varepsilon_\infty\left[1+\left(\frac{1}{\varepsilon_\infty}-1\right)e^{\left(-4D_w/d_p\right)}\right]-\varepsilon_m$, where ε_∞ is the nominal perfectly fixed bed porosity without an Al mesh, d_p is the diameter of the assumed-spherical sorbent pellets, ε_m is the volume fraction taken up by the Al mesh, and D_w is the local distance to the nearest wall. The latter is calculated with a modified Eikonal equation (Fares and Shroder 2002): $\nabla G\cdot\nabla G+\sigma_w G(\nabla\cdot\nabla G)=(1+2\sigma_w)G^4$

where G=1/D_w and σ_w =0.1 is a diffusion constant for numerical stability. In this model, inlets and exits are considered walls, since the experiment had fine meshes covering the columns, reducing the sorbent packing density at the inlets and exits in a way analogous to a wall. The permeability uses the BKZ model (Barenblatt, Zheltov and Kochina 1960) that is a function of porosity: $\kappa = d_p^2\varepsilon^3/(150(1-\varepsilon^2))$. The idealized porosity infinitely far from any walls is 37% of the volume, with 8% of the remaining 63% being taken up by the Al foam (ε_∞ =0.45 and ε_m =0.08), so that at the walls the porosity is 92%. Note for this small-scale setup, the minimum porosity is 0.385, slightly larger than ε_∞-ε_m. The Al foam, brazed to the canister walls, is, based on Fig. (8) above, assumed to have a thermal conductivity equal to ~46% of normal Al or 92 W m^{-1} K^{-1}. The pressure drop across the columns is primarily a function of geometry and turns out to be quite sensitive to the porosity and permeability models. The above models result in a pressure drop of ~170 Pa, compared to the experiment value of ~164 Pa, while using ε_∞ =0.465 gives a ~140 Pa pressure drop.

The wet inlet and dry inlet concentrations are held constant at 0.52 and 10^{-10} mol m^{-3}, respectively. The outlet pressure is held constant at the measured value of 14.2 psi, while the inlet temperature for the dry and wet flow use different functions $T_{in}(t)$ that are half-cycle averages of the experimental data (these T_{in} functions can be seen in the temperature results shown in Fig. 18).

The inlet boundary conditions for the porous fluid flow are a volumetric flow of 9.998 L/min divided by the mean inlet porosity; the flow needs to be normalized in this fashion since the problem starts at the bed inlet and thus the interstitial velocity is appropriate. The flow is initialized with a small axial velocity. On the other hand, the velocity field used by the heat transport equation is the superstitial velocity, so that $u = u_i\,\varepsilon$. The heat flux between the flowing gas and the Al canister is 16.8 W m-2 K-1, while between the canister and the air it is 1.1 W m-2 K-1. For the dilute species transport and heat transport equations, the exits are set to outflow. A ramp for small concentrations is applied to the pressure used to calculate the equilibrium loading, q^*. Similarly, the inlet concentration is ramped up over time. These ramps are applied solely for numerical stability; the results do not change.

First, a stationary solution is determined first, in order to get good initial conditions for the solver. Then an unsteady solution is solved. Every half cycle, the boundary conditions are switched and the unsteady calculation continued. COMSOL uses a parallel sparse direct linear (PARDISO) solver that exploits multithreaded parallelism.

The model discussed here is preliminary and simplistic, since its goal was to determine the applicability of COMSOL to the project. For example, a coarse grid, shown in Fig. 17, was used; the calculations are not expected to be temporally or spatially converged. Fig. 18 shows the temperature results at the end of 42 simulated 15-minute half-cycles compared to the last two half-cycles of the experiment. In the simulation, the wet exit flow initially undershoots, while the dry exit flow overshoots. Note the inflowing dry air is ~1.5K warmer than the inflowing wet air and has a different temporal shape. The cause of the ~0.2K mismatch between the wet inflowing air and dry exiting air and the ~0.4K mismatch between the dry inflowing air and the wet exiting air is unknown, but it may be related to the fact that the Al holder serves as a heat sink to the warmer incoming dry air, while the incoming wet air is closer to ambient temperature. The dry flow, as it removes water from the silica gel sorbent, cools by ~1.4K. The wet flow, as it deposits water on the sorbent, heats up by ~1.5K. This slight asymmetry is due to the shorter 'dis-

tance of run' for the hot flow: the wet flow has the whole column for the water to be adsorbed, while the desorbing dry flow, since the bed is not fully saturated, only finds water to pick up closer to the exit.

Fig. 19 shows the water concentration results from the simulation. It is evident that ~30 half-cycles are required to reach a quasi-steady state; the experiment was run much longer than this. The concentration at the wet inlet,

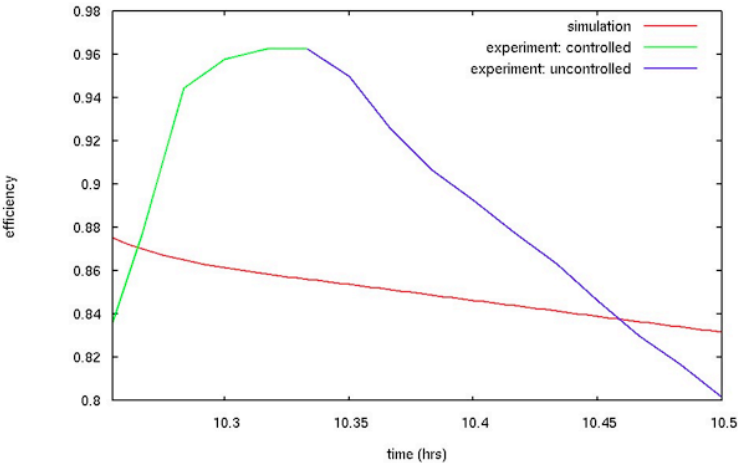

Figure 20. Efficiency, η, of the simulation compared to experiment over the last half-cycle. *During the 'controlled' period of each half-cycle, the dew point measuring device is calibrating, so the resulting concentration and partial pressures are uncertain.*

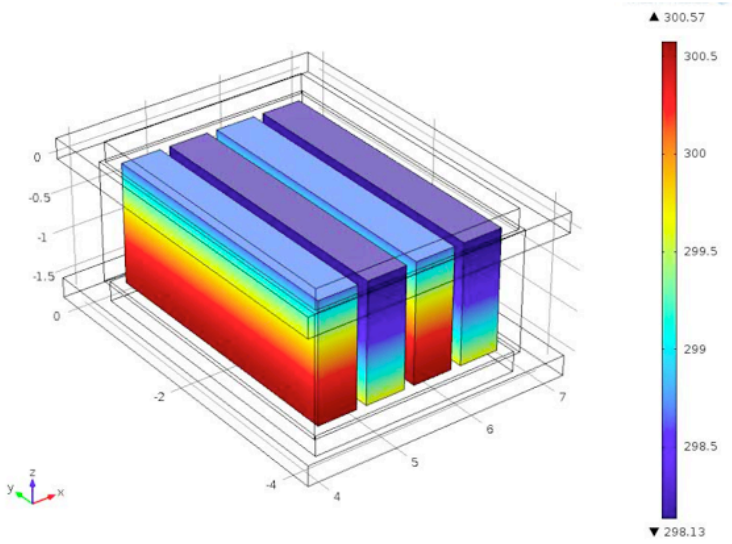

Figure 21. Temperatures (in K) on the bed surfaces at the end of the simulation. *Counting from left to right, columns 1 and 3 have wet air flowing downward and columns 2 and 4 have dry air flowing upward.*

when it becomes the dry exit, does not drop to zero in the short duration of a half-cycle. The wet flow concentration drops by ~0.44 mol m-3 before exiting the column, while the dry flow concentration increases by only ~0.31 mol m-3. This is in-line with the larger temperature change for the wet flow described above.

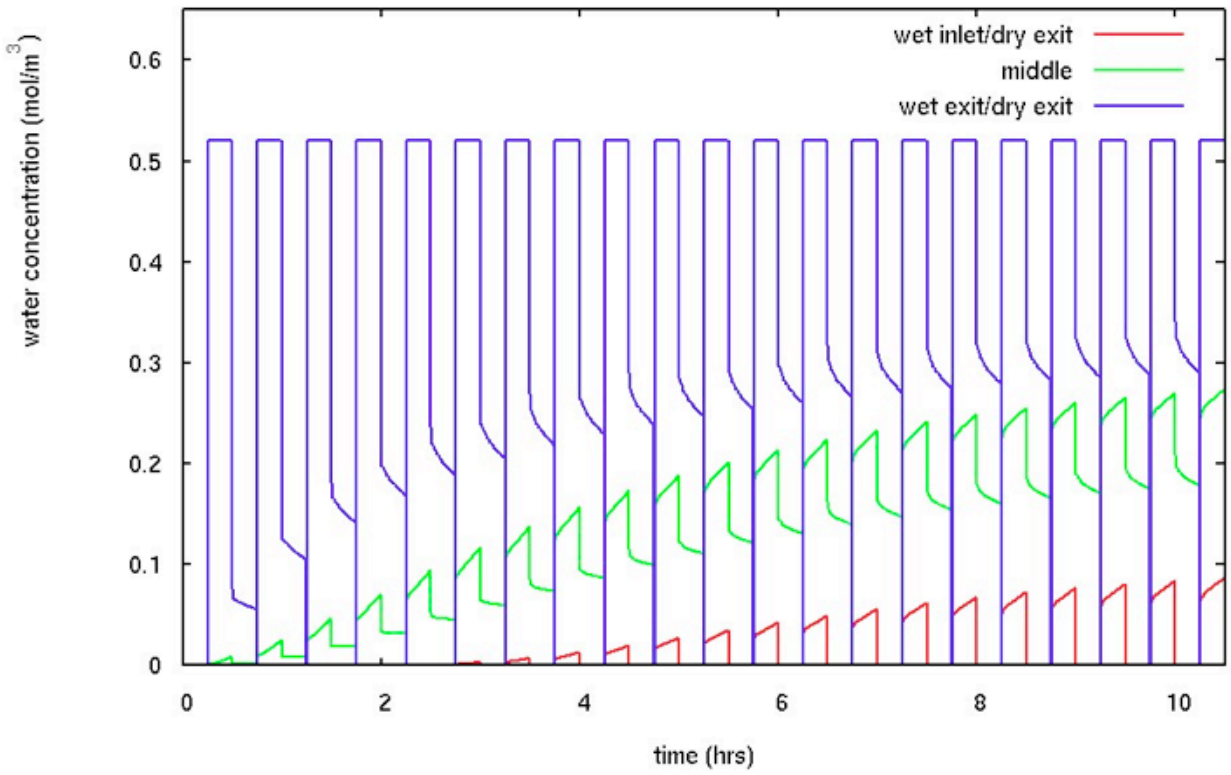

Figure 19. Water concentrations from the simulation. *The values are taken from the centerline. The 'middle' point is at the axial center of the bed.*

Converting the change in concentration into an efficiency, $\eta=1-P^{H2O}{}_{out}/P^{H2O}{}_{in}$ gives the results shown in Fig. X4. While the dew point monitor is calibrating (shown in green in Fig. X4), the results are unreliable. Note the function used to invert dew point temperature to partial pressure for Fig. X4 is not the same as is used elsewhere in this paper; thus, the efficiencies are somewhat lower. The simulation has a lower average efficiency overall. The rate of increase in the concentration coming out the exit throughout a single half-cycle is also too large in the simulation, so that the efficiency at the end of each half-cycle is actually too large; that is, the red curve in Fig. X3 should be flatter and and lower.

The temperatures on the surfaces of the four columns are shown in Fig. 20. Note that the Al holder (shown in outline in Fig. X5) is very nearly isothermal at ~299.25 Km with a slight asymmetry of ~0.03 K from the desorbing to adsorbing sides. Comparing this to the ambient ~298.75 K, this is consistent with the above discussion that heating slightly dominates cooling. The left-most column in Fig. 21 has wet air flowing downward that is getting heated as the H2O gets adsorbed onto the pellets, while the right-most column has dry air flowing upward that is getting cooled as the H2O gets desorbed from the pellets. This highlights the importance of accurately measuring the ambient temperature, or the holder temperature itself if it is insulated, in future experiments.

2. Results and Discussion

The first out-of-the-box attempt at using COMSOL Multiphysics to model the IBD process has resulted in a favorable match to data, at least in temperatures. Concentration is not matched as well, but this could be do to a number of reasons, from how the data was acquired (compared to the simulation) to variability in physical parameters (e.g. sensitivity to the axial dispersion coefficient, DL, used isotropically in the dilute species transport equation, has not been investigated). Further work will focus on modeling a thermally unlinked bed, which uses a plastic holder, as well as larger scale, higher flow rate experiments. Barring unforeseen issues with those models, COMSOL should be a useful tool to explore design space for ARREM IBD.

V. Microlith® Adsorber Model Development

Precision Combustion, Inc. (PCI), via NASA-sponsored projects, has been developing regenerable Microlith®-based adsorber modules for the separation of air constituents such as humidity, CO2, and trace contaminants to function in either closed or open loop operations. The Microlith® adsorbers use a patented technology developed by PCI to coat expanded metal with zeolite sorbent crystals to produce a structured sorbent. An advantage of this configuration is that can be thermally regenerated by passing a current through the electrically-resistive expanded metal. Previous developmental work has focused on testing individual Microlith®-based adsorber modules for residual humidity removal, trace contaminant removal, and CO2 removal. The most recent developmental work evaluated the integrated operation of the residual humidity removal and CO2 removal adsorber modules. The adsorber design concept is shown is Fig. 22 (Perry et. al. 2009).

The full scale water Microlith "Jelly Roll" was modeled for comparison with exit axial velocity measurements. The COMSOL Multiphysics modeling package, with porous media equations and axisymmetric geometry, was used. Inspection of model results helped to identify a probable bypass flow of the sorbent bed occurring at the left and right ends of the sorbent jelly roll as oriented in Fig. 22. Testing verified that the previous insulation, alumina paper, was not thick enough nor compliant enough to prevent flow between the edge of the jelly roll and the ceramic plate..

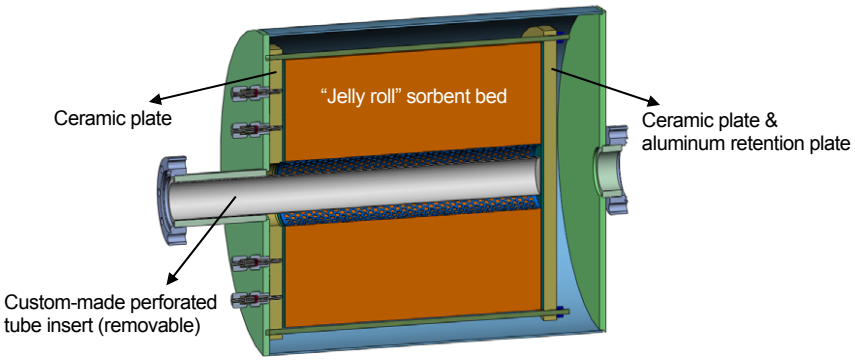

Figure 22. Internal cross-section view of the Microlith-based radial flow adsorber design concept.

A. Modeling and Simulation

Air properties at 20 C and 1.002 bar were assumed for the input and sorbent volumes. Since flow mapping was the primary concern, adsorption physics were neglected for the present. Porosity was assumed to be 0.5. Boundary conditions at the inlet was designed as standard volumetric rate and at the outlet as no viscous stress. The inlet volumetric flow rate was held constant at 600 L/min. Permeability was varied as 9.8e-10 m^2, 9.8e-9 m^2 , and 9.8e-8 m^2 for this study in order to match test measurements of overall pressure drop. The model geometry is further described in Fig. 23.

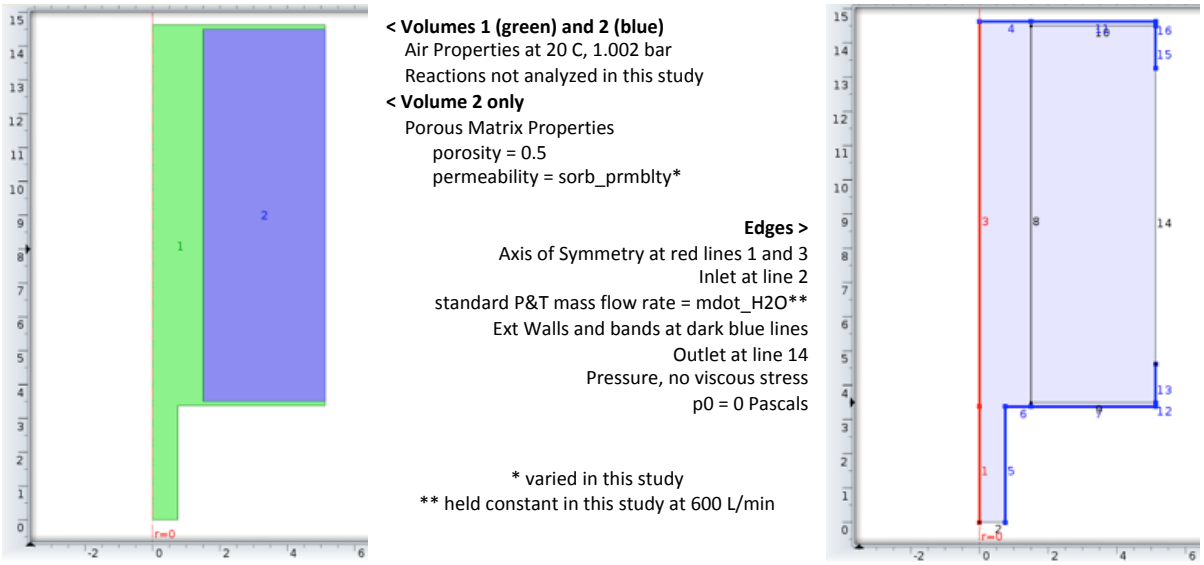

Figure 23. H_2O Microlith Model Geometry

B. Results and Discussion

The jelly roll exit velocities for the three sorbent permeabilities modeled are shown in Fig. 24. Note that a flow rate of zero ft/min was both simulated and measured below 4.7 inches and above 13.2 inches. Immediately adjacent to the insulation wrap, flow rates of approximately 50 ft/min were measured. This correlates well with the simulated velocities in Fig. 24 using the highest value of 9.8e-8 m^2 for permeability. Figure 25 provides the 3-D velocity mapping of the jelly roll for the lowest and highest permeability values.

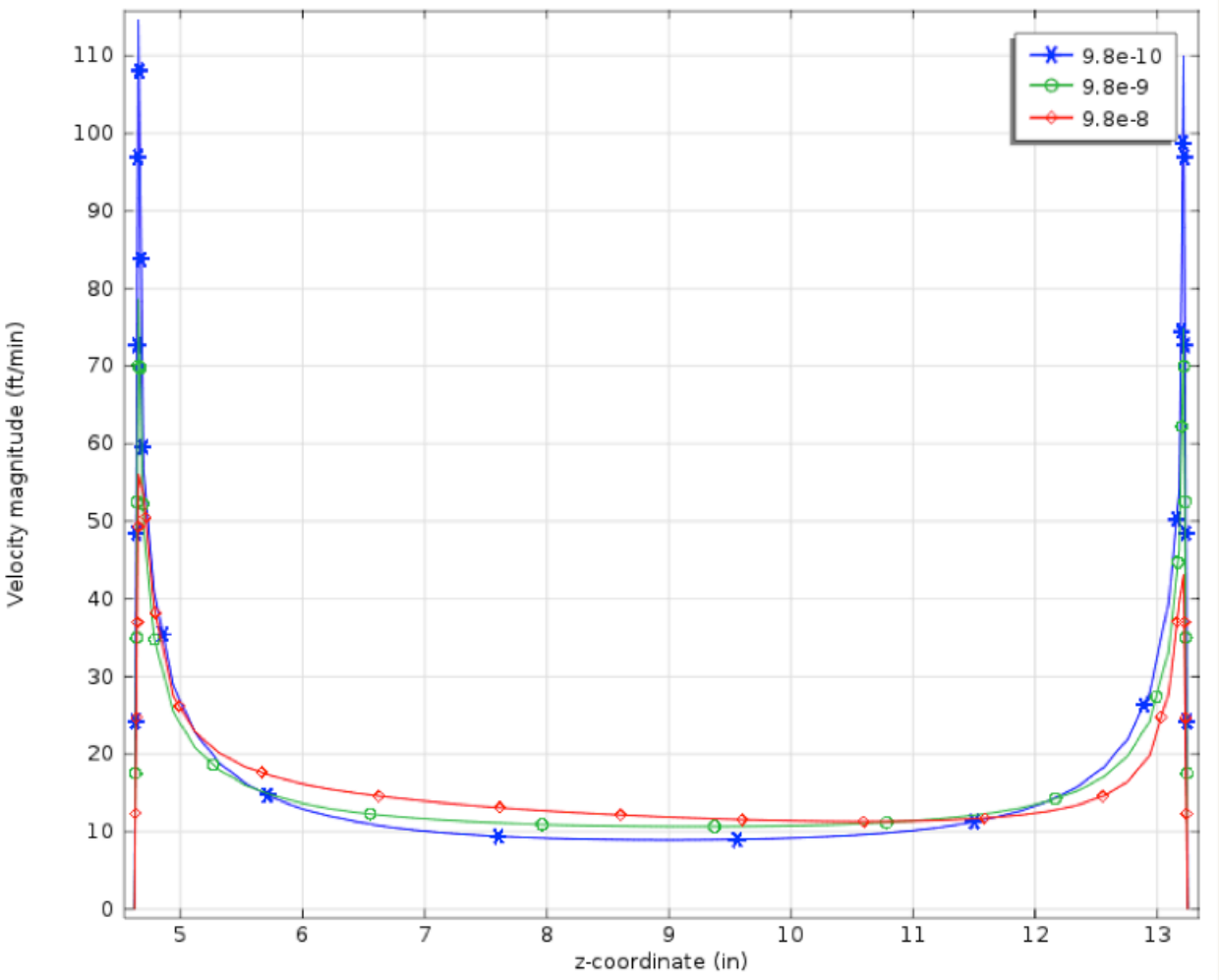

Figure 23. Jelly Roll Exit Velocities

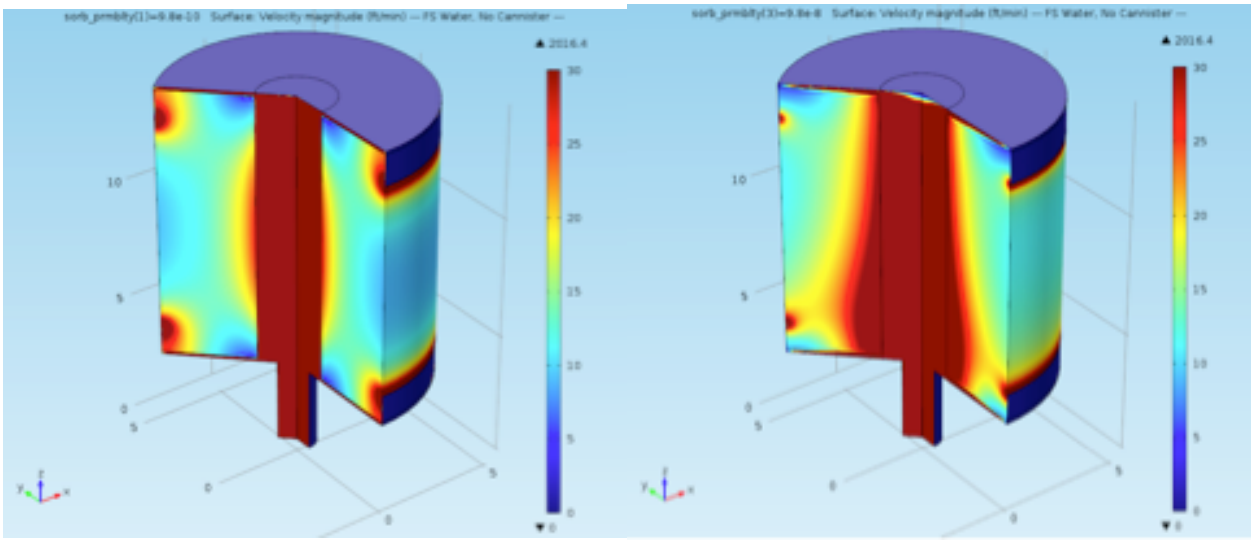

Figure 25. 3-D Velocity Mapping of the Jelly Roll for the Lowest (left) and Highest (right) Permeability Values

As discussed in the companion design paper, this analysis provided important insight leading to successful corrective action for the flow channeling problem. Further uses of this model will be to map flow maldistribution following corrective action. With the addition of adsorption physics, this model will provide a means for optimization of cyclic parameters for this particular hardware, and allow for design optimization studies for new Microlith designs.

VI. CARE Test Facility Vacuum System Analysis

A. Introduction

This section describes the fluid analysis of the Common Atmosphere Revitalization for Exploration (CARE) test facility vacuum piping system. The CARE concept is to develop a common adsorption canister for applications ranging from portable life support systems to long-term habitats. The objective is to reduce hardware development costs and increase reliability via long-term testing and operational experience. The vacuum system will be used for desorption of CO_2 and water from the fixed bed in a proof of concept test. The purpose of the analysis is to develop models to predict the vacuum conductance of the piping system. The resulting models will be coupled for the 2D fixed bed analysis. The detailed COMSOL 3D vacuum model was used as a virtual testbed to verify a simplified 1D pressure drop model using Mathcad.

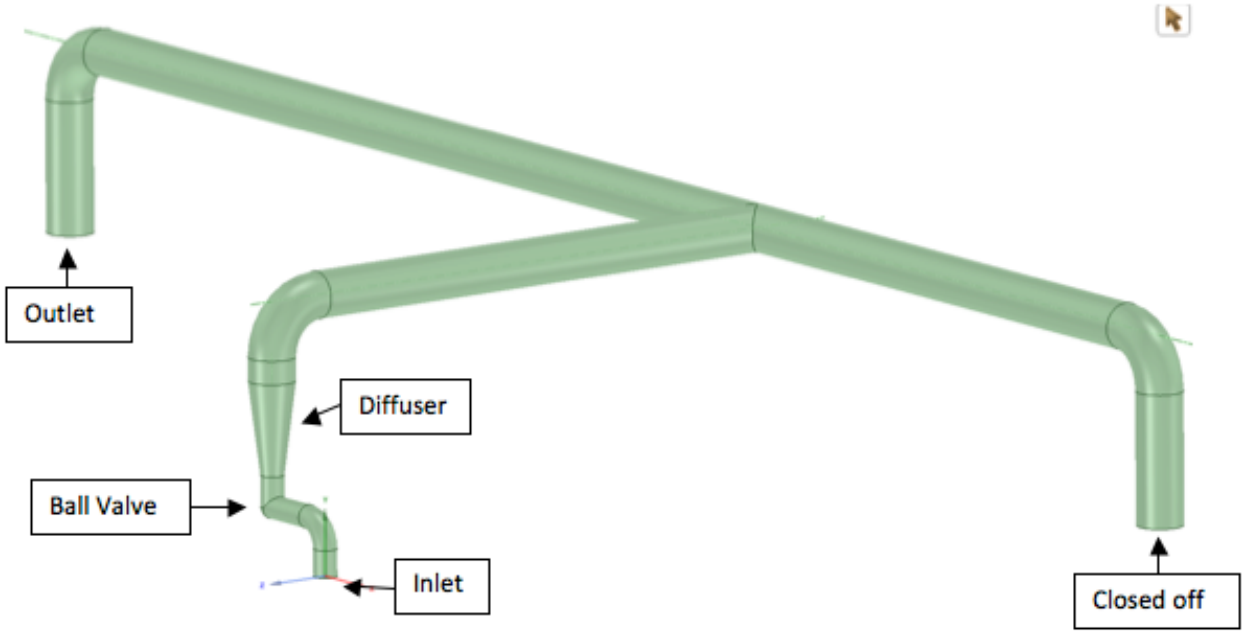

Figure 26. Vacuum Piping System

B. Experimental

The inlet and outlet of the piping system are illustrated in Figure 26. The piping starts as 3" diameter pipe and increases to 6" diameter after the valve. The valve internals were simplified and modeled to match the test hardware as closely as possible.. The volume and surface, where the pipes bend and are joined, were simplified to avoid meshing errors. The 3D model was created using SpaceClaim and imported to COMSOL.

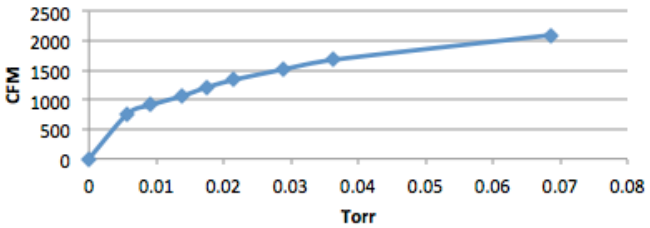

Figure 27. Pump Curve

The physics and boundary conditions for the model were determined by a previous test conducted with the same vacuum piping and pump configuration. For this test, a controlled mass flow of nitrogen was injected into a fixed

bed open to the vacuum system. Various mass flows were injected and pressure and volumetric flow rates were recorded for each case. The vacuum pump curve created from these data is shown in Fig. 27.

C. Modeling and Simulation

1. COMSOL Model

The vacuum flow regime was determined first to identify the appropriate flow equations. For inlet pressures greater than 0.064 torr, as expected for CARE test conditions, the Knudsen number was calculated to be less than 0.01, indicating that the flow is in the continuum regime in the 3 inch pipe. The largest volumetric flow rate and the area at the outlet were used to determine the velocity and calculate the Reynolds number of the piping system. The highest Reynolds number was $Re = 73$ indicating that the flow is in the laminar regime.

The physics used in COMSOL was Single Phase Flow-Laminar Flow-Weakly Compressible. The dynamic viscosity was defined as a constant of .000017436 Pa•s. An initial condition of 1 Pa was assumed for the entire volume.

The boundary condition for all walls was assumed to be the no slip condition except for the inlet and outlet. The inlet was given a pressure boundary condition which was varied for each case. The outlet condition was interpolated from the pump curve data, which was entered into COMSOL as a static pressure curve.

2. Mathcad Model

A simplified 1D pressure drop model was created in MathCad and correlated with the COMSOL 3D model. Density was calculated using the Ideal Gas Law EOS as a function of pressure. The pipe system was divided into straight pipes and bends and the head losses were calculated at each component. The equations used for each region were derived based on fully developed Poiseuille flow in round pipes; these are summarized below.

Poiseuille's Law
$$P_1 - P_2 = \rho\left[\frac{V_2^2 - V_1^2}{2} + \frac{V^2}{2}\left[\frac{64}{Re}\frac{L}{d}\right]\right] \tag{14}$$

Entrance Region
$$P_1 - P_2 = \left(\frac{P_1+P_2}{2RT}\right)\left[\frac{V_2^2 - V_1^2}{2} + \frac{(V_1+V_2)^2}{8}[64 * .06]\right] \tag{15}$$

Straight Pipes
$$P_1 - P_2 = \left(\frac{P_1+P_2}{2RT}\right)\left[\frac{V_2^2 - V_1^2}{2}\right] + \left[\frac{32\mu L(V_1+V_2)}{2d^2}\right] \tag{16}$$

Bends
$$P_1 - P_2 = \left(\frac{P_1+P_2}{2RT}\right)\left[\frac{V_2^2 - V_1^2}{2} + \frac{1}{2}\frac{64}{Re}V^2\frac{\pi R_b}{D}\frac{\theta}{180} + \frac{1}{2}k_b V^2\right] \tag{17}$$

D. Results and Discussion

The 3D COMSOL model and the 1D Mathcad model showed very similar results for the same boundary conditions and assumptions. The 1D model used compressible equations where possible to achieve as close a match a possible to the compressible COMSOL model predictions.

The outlet pressure comparison from both models is very favorable at lower pressures, though some divergence is observed at higher inlet pressures. Figure 28 shows the outlet pressure comparison. Similar results for mass flow are observed, with a very favorable comparison at lower pressures, and some divergence at higher pressures.

The detailed COMSOL 3D vacuum model uses a small amount of computing resources to solve for the cases used in this analysis. However, coupling the 3D vacuum system COMSOL model with the 2D fixed bed COMSOL model would require a large amount of computing power since the packed bed analysis is complex with multiple physics solved simultaneously. Alternatively, a reasonable correlation using the empirical 1D equations as shown here may be used for the vacuum system, reducing the required computing resources.

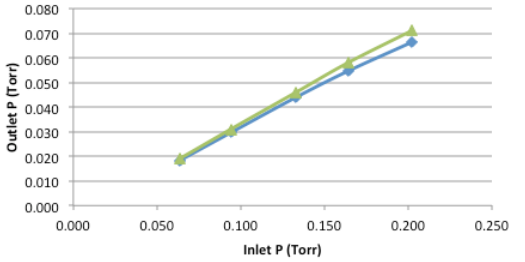

Figure 29. Outlet Pressure vs. Inlet Pressure

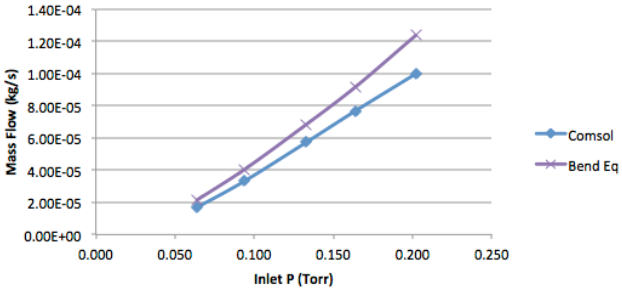

Figure 30. Mass Flow vs. Inlet Pressure

VII. Conclusions

The need for atmosphere revitalization systems that are optimized with respect to performance, resources, and is necessitated by the aggressive new missions planned by NASA. With NASA budgets remaining flat, innovative approaches to new system development are required. This paper presents such an approach for the AES ARREM project, where testing is supplemented with modeling and simulation to reduce costs and optimize hardware designs. In this paper, we have discussed the empirical determination of mass transfer coefficients using accurate fixed bed models in 1D and 2D, the optimization of heat transfer for development of a Isothermal Bulk Desiccant (IBD) and the application of the fixed bed model in 3D to simulate a cyclic IBD sub-scale test. Studies of the Microlith® Adsorber flow pattern have been used to troubleshoot performance problems and to obtain a successful solution to the flow maldistribution. Finally, the groundwork has been laid for a Common Air Revitalization for Exploration (CARE) test by developing the appropriate, simplified vacuum system equations and verifying them against a detailed 3D multiphysics simulation.

The efforts represented here will be continued to support the design of Atmosphere Revitalization systems under the ARREM project. These modeling and simulation efforts are expected to provide design guidance, system optimization, and troubleshooting capabilities for atmosphere revitalization systems being considered for use in future exploration vehicles.

VIII. References

1 **NASA**. Human Exploration & Operations (HEO). 2012).

2 **Mohamadinejad, H., Knox, J.C. and Smith, J.E.** Experimental and Numerical Investigation of Adsorption/ Desorption in Packed Sorption Beds under Ideal and Nonideal Flows. *SEPARATION SCIENCE AND TECHNOLOGY*, 2000, **35**(1), 1-22.

3 **COMSOL**. COMSOL Multiphysics®. 2009).

4 **Perry, J., Howard, D.F., Knox, J.C. and Junaedi, C.** Engineered Structured Sorbents for the Adsorption of Carbon Dioxide and Water Vapor from Manned Spacecraft Atmospheres: Applications and Testing 2008/2009. *International Conference on Environmental Systems* (SAE, Savannah, GA, 2009).

5 **Corporation, E.A.** Duocel® Aluminum Foam.

6 **Fares, E. and Shroder, W.** A Differential Equation for Approximate Wall Distance. *Intl. J. Num. Meth. Fld*, 2002, **39**, 743-762.

7 **Barenblatt, B.I., Zheltov, I.P. and Kochina, I.N.** Basic concepts in the theory of seepage of homogeneous liquids in fissured rocks. *J. Appl . Math. Mech.*, 1960, **PMM 24**, 1286-1303.